A scatter correction method of CBCT via CycleGAN and forward projection algorithm

Tianxu Tang[a], Wei Zhang[a], and Weiqi Xiong[a]

[a] United Imaging Healthcare, Shanghai, China

ABSTRACT

Scatter artifacts is one of the limitations of cone-beam computed tomography(CBCT) image quality, this paper proposed a novel scatter correction method for CBCT via combining the deep learning and forward projection algorithm. This method can be mainly divided follow steps: Firstly, raw projections were used to reconstruct raw CBCT via FDK algorithm, and then the raw CBCT was processed by CycleGAN network to generate synthetic CT, after that the synthetic CT was used to forward projection based on the Beer's laws to generate scatter free primary projections. The raw scatters can be estimated via subtracting the primary projections from the raw projections, and then a median and low-pass Gaussian filter was used to smooth the raw scatters. Finally, The scatter corrected projections can be acquired by subtracting the filtered scatters form raw projections. The study results of pelvis and chest validated the effective of proposed correction method in reducing scatter artifacts of CBCT. Compared with uncorrected CBCT and CBCT corrected by scatter kernel superposition(SKS) method, the proposed method can more effectively improve the quality of reconstructed CBCT, reducing the CT number errors and increasing contrast-to-noise(CNR) and so on. All results show that this method has strong scatter artifacts restriction ability, so it has significant promising for clinical application.

Keywords: CBCT, scatter correction, CycleGAN, forward projection

1. INTRODUCTION

Cone-beam CT (CBCT) has been widely used in image-guide radiation therapy, it can provided accurate patient position, and also can track the tumor positon in therapy. But as the existing of scatter signals in CBCT, it will lead to strong noise and CT number errors. This is one of reasons to limit the application of CBCT in dose calculation, adaptive radiation therapy and so on. Scatter correction technology for CBCT has been widely study, those methods can be mainly divided three categories: software-based,[1–4] hardware-based[5,6] and software-hardware hybrid methods.[7–11] In earlier study, many hardware-based methods been proposed, such as anti-scatter grid method, air gap method and so on. Software-based mainly contains Monte Carlo, deep learning and SKS methods. Furthermore, there are also some methods combined the hardware and software, those study usually include beam stop array, primary modulation method and so on. Above scatter correction methods mainly via direction measurement or theoretical calculation to estimate scatter, considering the characteristic of existing planning CT in radiation therapy, there are also methods estimate scatter signals via planning CT forward projection and then subtracted it from raw projections.[12–15] Nui et al[12] via rigid registration of the planning CT with CBCT, and then forward projection process be used in planning CT to acquire primary projections, so the scatter signals can be estimated easily and be smoothed. To further decrease the estimated scatter errors, they also used some improvement technologies such as deformable registration, gas pocket matching in this method. As the mismatching of CBCT with planning CT, it will leads serious errors for scatter estimation, Cui et al[16] used local filtration technique for the estimated scatter signals to improvement the accuracy of scatter estimation furthermore.

Nui and Cui's method just can used in those situation there are planning CT and it significantly rely on the accuracy of registration. In this paper, We proposed a novel scatter correction method via combine the deep learning and forward projection technique. A CycleGAN deep learning network was used to convert the CBCT to synthetic CT, and then use synthetic CT to generate primary projections, and estimating scatter signals. Our

Further author information:
Tianxu Tang: E-mail: tangtianxu0815@gmail.com

7th International Conference on Image Formation in X-Ray Computed Tomography,
edited by Joseph Webster Stayman, Proc. of SPIE Vol. 12304, 1230418
 · 0277-786X · doi: 10.1117/12.2647147

method has significant advantages that it didn't need any prior information, so the application regions are more extensive, and proposed method also avoided the scatter estimation errors bring by registration.

2. METHODS

2.1 Generating Synthetic CT

We used CycleGAN network[16] as basic deep learning network to convert raw CBCT to synthetic CT, it used two generators and discriminators to convert images between two cycle networks. We used a U-net architecture for generators and a patchGAN for discriminators. Generators are used to generate synthetic CT, while discriminators are used to distinguish real or fake data, Fig2 shows the architecture of CycleGAN network in this paper, it mainly include two cycles. In cycle one, CBCT is converted to synthetic CT via generator G_1, and discriminator D_2 is used to discriminate synthetic CT and real fan-beam computed tomography(FBCT) to restrain generator G_1, generator G_2 is used to generator synthetic CBCT from synthetic CT. In cycle two, FBCT is firstly converted to synthetic CBCT by generator G_2, while discriminator D_2 discriminates between synthetic CBCT and real CBCT, and the same time synthetic CBCT is converted to synthetic CT using generator G_2. We used 24 patients dataset as training, 5 patients dataset as validation, and 2 patients dataset as test to train CycleGAN network. Every patient contains 270 CBCT slices with 512x512 axial pixel and thickness 1mm, the corresponding FBCT also was resampled to same size with CBCT.

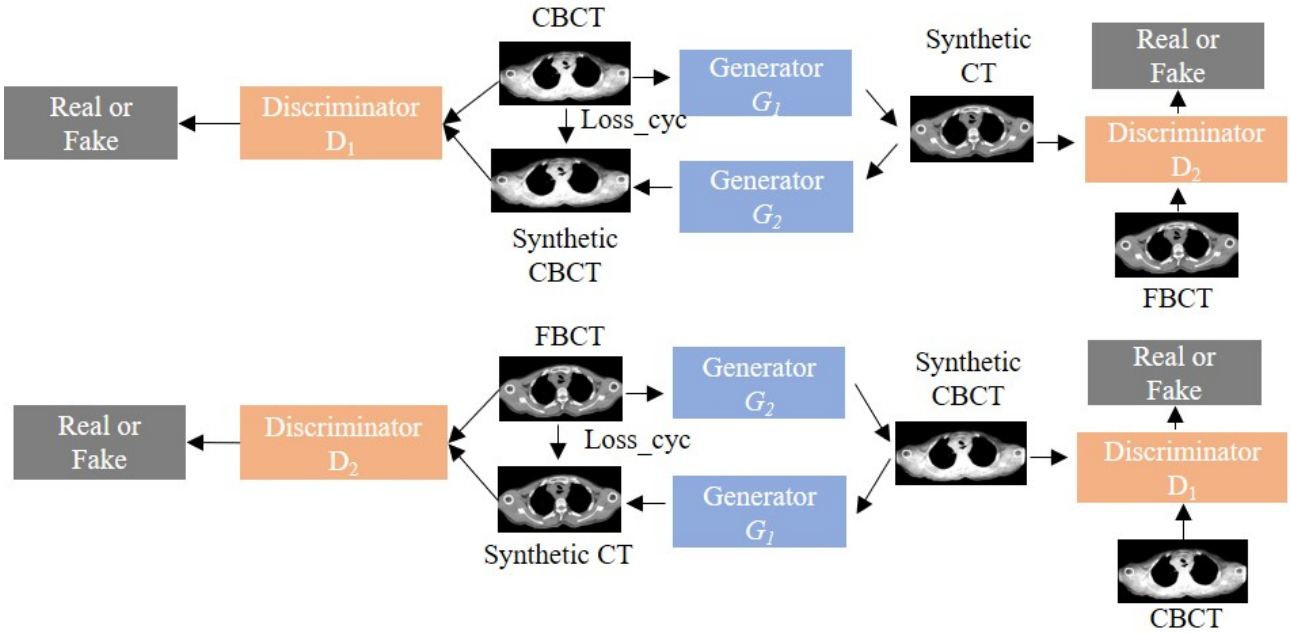

Figure 1. The architecture of CycleGAN network in this paper.

2.2 Scatter Estimation

The work flow of proposed scatter correction method as show in Fig1. Raw CBCT images were reconstructed firstly using standard FDK algorithm, and then the CBCT images were used to generate synthetic CT images via CycleGAN network. In forward projection procedure, HU number of synthetic CT firstly was transformed to corresponding water density, scatter free primary projections were acquired via forward projection of synthetic CT images based on Beer's law. In traditional scatter correction using deep learning directly, the high-frequency errors can not be tolerant, but in our case only the low-frequency signals of synthetic CT are used, so our method has some tolerance for high-frequency errors of synthetic CT. To improve the calculation times and save memory space, the primary projections and raw projections were downsampled from 1024×1024 to 256×256. When subtracting estimated scatter form raw projections, the scatter signals will be upsampled firstly back to

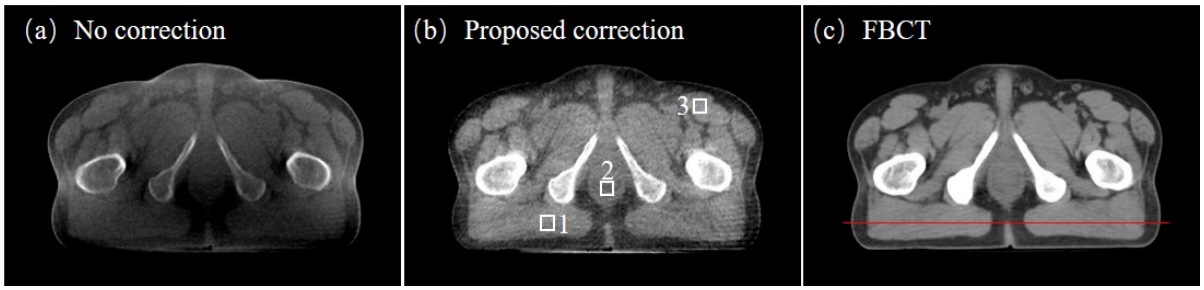

Figure 2. The pelvis study with different way: (a)no correction, display window:[-200 400]; (b)with proposed correction, display window:[40 400]; (c)ground truth FBCT, display window:[40 400].

1024×1024. For every projection angle, subtraction of primary projections from raw CBCT projections gives the raw scatter projection images. Synthetic CT maybe has some slight errors, so there were some mismatching between raw CBCT projections and primary images of forward projection, and the low frequency characterize of scatter signals, a median filter(size 45-by-45 pixels) and a low-pass Gaussian filter(size 51-by-51 pixels) was used to smooth raw scatter projection images. Finally, subtracting smoothed scatter from raw projections, and then using subtracting results to reconstructed via FDK algorithm.

2.3 Evaluation Metrics

To evaluate the performance of proposed correction method, using contrast and contrast-to-noise (CNR) as the evaluation metrics, the contrast calculated as:

$$Contrast = HU_r - HUs \tag{1}$$

the CNR calculated as:

$$CNR = \frac{HU_r - HUs}{\sqrt{\sigma}} \tag{2}$$

here HU_r is the mean of selected region, HU_s is the mean of surrounding area, σ is the standard deviation of selected region.

3. RESULTS AND DISCUSSION

We performed our study on United-Imaging uRT-linac 506c, it contains an advanced MV-CBCT and FBCT system. The reconstructed FBCT images had a pixel size of 512×512×90 and voxel size of 0.97mm in axial plane and 3mm in longitudinal direction, while the CBCT images had a pixel size of 512×512×270 and voxel size of 0.78mm in axial plane and 1mm in longitudinal direction. To enlarge the field of view of MV-CBCT imaging, the flat detector was shifted by 90mm, and the reconstruction system of uRT-linac 506c contains strong denoising process. Fig3 shows a pelvis study, it contains without correction CBCT, proposed correction CBCT and ground truth FBCT. In the pelvis case, the HU number of CBCT corrected by proposed method has significant increase than without correction CBCT, and the serious artifacts in without correction images had been improved via proposed method. The red line profile showed in Fig4 also demonstrate the effective of our method, and it is more nearing the FBCT compare with without correction. To quantitatively evaluate the performance of our method, three ROIs were chosen to calculate the CNR and contrast number as show in table1. In the selected ROIs, the CNR and contrast of three areas had obvious increasing. To further evaluate proposed scatter correction method, Fig5 shows the CBCT images of a chest data corrected by proposed method and SKS correction method. SKS scatter correction has been wildly study and used in commerce, because it has good performance and fast calculation, and don't need any other hardware equipment. From the chest performance at axial, coronal and sagittal plane, we can see that the contrast and HU uniformity of CBCT corrected by proposed correction has significant improvement compared with SKS correction.

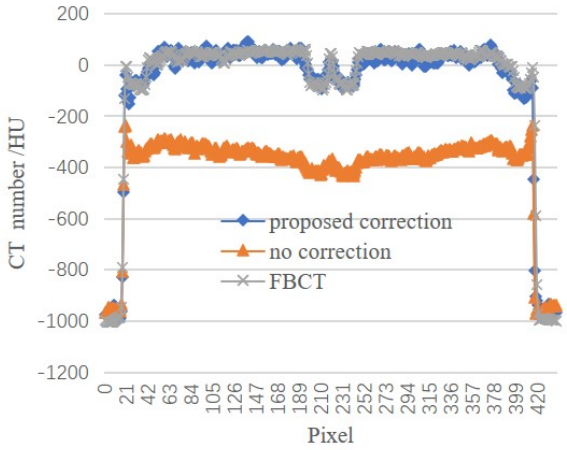

Figure 3. 1D horizontal profile along the solid line drawn in Fig2(c).

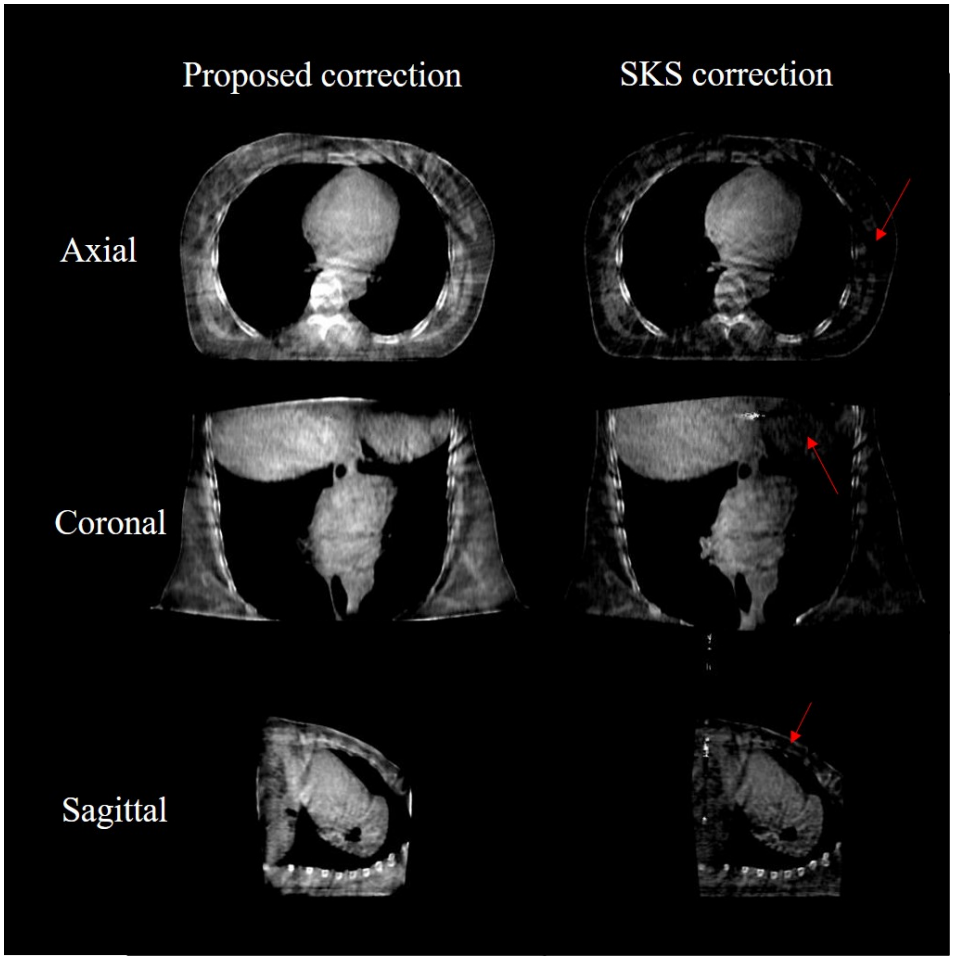

Figure 4. The chest study with proposed and SKS correction. Left column is proposed correction, right column is SKS correction.From top to bottom is axial, coronal and sagittal plane. All images with display window:[40 400].

Table 1. Contrast and CNR of selected regions

Method	Metrics	ROI1	ROI2	ROI3
Proposed correction	Contrast	104	80	121
	CNR	25.22	17.45	31.4
Without correction	Contrast	52	48	11
	CNR	18.44	13.9	3.5

REFERENCES

[1] Jarry, G., Graham, S. A., Moseley, D. J., Jaffray, D. J., Siewerdsen, J. H., and Verhaegen, F., "Characterization of scattered radiation in kv cbct images using monte carlo simulations," *Medical Physics* **33**, 4320–4329 (2006).

[2] Maslowski, A., Wang, A., Sun, M., Wareing, T., Davis, I., and Star-Lack, J., "Acuros cts: A fast, linear boltzmann transport equation solver for computed tomography scatter – part i: Core algorithms and validation," *Medical Physics* **45**(5) (2018).

[3] Liang, X., Chen, L., Nguyen, D., Zhou, Z., Gu, X., Yang, M., Wang, J., and Jiang, S., "Generating synthesized computed tomography (ct) from cone-beam computed tomography (cbct) using cyclegan for adaptive radiation therapy," *Physics in Medicine & Biology* **64**(12), 125002 (2019).

[4] Niu, T., Sun, M., Star-Lack, J., Gao, H., Fan, Q., and Zhu, L., "Shading correction for on-board cone-beam ct in radiation therapy using planning mdct images," *Medical physics* **37**(10), 5395–5406 (2010).

[5] Shen, S. Z., Bloomquist, A. K., Mawdsley, G. E., Yaffe, M. J., and Elbakri, I., "Effect of scatter and an antiscatter grid on the performance of a slot-scanning digital mammography system," *Medical physics* **33**, 1108–1115 (2006).

[6] Siewerdsen, J. H., Moseley, D., Bakhtiar, B., Richard, S., and Jaffray, D. A., "The influence of antiscatter grids on soft-tissue detectability in cone-beam computed tomography with flat-panel detectors: Antiscatter grids in cone-beam ct," *Medical physics* **31**(12), 3506–3520 (2004).

[7] Ning, R., Tang, X., and Conover, D., "X-ray scatter correction algorithm for cone beam ct imaging," *Medical physics* **31**(5), 1195–1202 (2004).

[8] Min, J., Pua, R., Kim, C., Park, M., Lee, J., Ye, S.-J., and Cho, S., "A weighted rebinned backprojection-filtration algorithm from partially beam-blocked data for a single-scan cone-beam ct with hybrid type scatter correction," *Medical Physics* **46**(3), 1182–1197 (2019).

[9] Choi, Y.-W., Choi, J.-G., Kim, Y.-s., Park, H.-S., and Kim, H.-J., "Scatter characterization using a beam-stop-array algorithm for digital breast tomosynthesis," *Journal of the Korean Physical Society* **63**(11), 2239–2246 (2013).

[10] Gao, H., Zhu, L., and Fahrig, R., "Virtual scatter modulation for x-ray ct scatter correction using primary modulator," *Journal of X-Ray Science and Technology* **25**(6), 869–885 (2017).

[11] Gao, H., Zhu, L., and Fahrig, R., "Modulator design for x-ray scatter correction using primary modulation: Material selection," *Medical physics* **37**(8), 4029–4037 (2010).

[12] Niu, T., Sun, M., Star-Lack, J., Gao, H., Fan, Q., and Zhu, L., "Shading correction for on-board cone-beam ct in radiation therapy using planning mdct images," *Medical physics* **37**(10), 5395–5406 (2010).

[13] Andersen, A. G., Park, Y. K., Elstrm, U. V., Petersen, J., and Muren, L. P., "Evaluation of an a priori scatter correction algorithm for cone-beam computed tomography based range and dose calculations in proton therapy," *Physics and Imaging in Radiation Oncology* **16**, 89–94 (2020).

[14] Yang, C., Wu, P., Gong, S., Wang, J., Lyu, Q., Tang, X., and Niu, T., "Shading correction assisted iterative cone-beam ct reconstruction," *Physics in Medicine & Biology* **62**(22), 8495 (2017).

[15] Cui, H., Jiang, X., Fang, C., Zhu, L., and Yang, Y., "Planning ct-guided robust and fast cone-beam ct scatter correction using a local filtration technique," *Medical physics* **48**(11), 6832–6843 (2021).

[16] Zhu, J.-Y., Park, T., Isola, P., and Efros, A. A., "Unpaired image-to-image translation using cycle-consistent adversarial networks," in [*Proceedings of the IEEE international conference on computer vision*], 2223–2232 (2017).